Development of an equivalent porous medium model for a tubular receiver equipped with Raschig Rings

RESEARCH ARTICLE | OCTOBER 06 2023

Development of an equivalent porous medium model for a tubular receiver equipped with Raschig Rings

Hossein Ebadi; Andrea Allio; Antonio Cammi; Laura Savoldi

AIP Conf. Proc. 2815, 070001 (2023)
https://doi.org/10.1063/5.0148833

Development of an Equivalent Porous Medium Model for a Tubular Receiver Equipped With Raschig Rings

Hossein Ebadi[1], Andrea Allio[1], Antonio Cammi[2], and Laura Savoldi[1, a)]

[1]*Dipartimento Energia "Galileo Ferraris", Politecnico di Torino, Corso Duca degli Abruzzi 24, 10129 Torino, Italy.*
[2] *Department of Energy, Politecnico di Milano, Via Lambruschini 4, 20156 Milano, Italy.*

[a)] Corresponding author: laura.savoldi@polito.it

Abstract. The porous insert has become one of the promising methods for heat transfer enhancement in many industrial applications ranging from small electronic devices to nuclear reactors, and large solar fields. For the assessment of such systems, the CFD numerical studies are usually employed by scientists to investigate the heat and mass transfer inside the region in micro or macro scales. Although micro studies are accurate and provide a detailed analysis of the process, they cannot be used for every study due to complex and costly computational resource they may demand for the case under study. Therefore, sometimes macro-scale simulations become more favorable thanks to the reduction in time and cost as well as the simplification over the morphology of the porous medium they offer. For these reasons, this study aims at developing a macro model for a novel porous disc made of Raschig Rings, to be applied to the tubular solar absorber for future simulations. The methodology devised in this study was to exploit detailed micro-scale simulations, achieving the macro properties and then developing a new equivalent macro model of a porous medium, based on the obtained properties. Numerical data indicated that when the developed macro model is compared to the micro simulations, the thermo-hydraulic results are in good agreement. Applying the macro model to a solar absorber working under linear Fresnel heating showed that the proposed porous disc could reduce the temperature rise on the tube wall by 40%.

INTRODUCTION

In many different applications where heat removal is an issue, such as electronic devices for instance [1], porous media and porous materials have shown promising effects on thermal efficiency augmentation with the increasing heat-transfer area, boosting thermal conduction, and improving convective heat transfer coefficient within the fluid flow regimes. In the field of Concentrating Solar Power (CSP), where a high flux of energy comes to the receivers, the thermal improvement could be a boon to the final energy generation process. In general, the thermal enhancement techniques can be applied through passive, active and hybrid methods, where, among the proposed models, passive techniques are the favorable option due to the less energy they use during the process [2]. The insertion of porous matrix is one of the common passive methods that forces a reduction in thermal boundary layer thickness, and an increase in the heat transfer area, producing higher thermal efficiency [3]. To take advantage of that, various porous materials and models have been developed by scientists [4,5] to increase thermal efficiency in solar CSP applications.

The modeling of the heat and mass transfer of fluids across a porous medium can be performed at the macroscopic or microscopic level. In the macroscopic or volume averaging approach, the porous matrix is treated as a homogeneous medium, neglecting small-scale details, while in pore-scale (or microscopic view) the dynamic behavior of the fluid in the porous medium is investigated based on macroscopic parameters determined on the micro-geometry of the system [6]. As a result, the 3D-detailed modeling of CSP receivers with porous inserts would require extensive computational resources and to achieve a good trade-off between computation time and quality of the results. The development of an equivalent model, representing the thermo-hydraulic of the porous medium, is then necessary. In this regard, scientists use the microscopic approach to describe the macroscopic parameters such as permeability, porosity, tortuosity, etc. of porous structures due to the ability to achieve detailed information of the materials [7]. A similar approach was tested by Cagnoli et al. [8] for the evaluation of an open volumetric air receiver enhanced with the

SolarPACES: Solar Power & Chemical Energy Systems
AIP Conf. Proc. 2815, 070001-1–070001-9; https://doi.org/10.1063/5.0148833
Published by AIP Publishing. 978-0-7354-4623-6/$30.00

porous structure where using a multi-scale numerical led to analyzing the entire receiver behavior. Avila-Marin et al[9] employed the commercial code STAR-CCM+ to firstly study the heat transfer coefficient between the air and volumetric air receiver with wire meshes with the detailed 3D CFD simulations (microscopic level) and then validate the results with a homogeneous equivalent model (macroscopic level). However, among those investigated, there are a few options that can be presented as a suitable case for linear gaseous CSP systems, while tubular absorbers still need further developments in the case of integration with porous media to reach a reasonable level in current CSP technology.

Porous metal matrices formed with Raschig Rings (RR) [10] have been already shown to be a viable solution for the power exhaust from gyrotron resonance cavities [11] when the cooling fluid is water. More recently, a planar mock-up equipped with RR on the back of the target surface for the external heating has been tested in a solar furnace at the Plataforma Solar de Almeria [12], confirming good thermal performances also when the cooling fluid is air and avoiding excessive detrimental effects on the receiver pressure drop. The detailed 3D numerical simulation of tubular receivers equipped with porous inserts made by RR for solar applications has been recently presented in [13] and [14], showing that the metal matrix is capable to significantly decrease the pipe temperature, thus decreasing the radiative and convective losses toward the environment, and at the same time increasing the useful heat flux to the fluid. Detailed simulations are usually precise; however, they are computationally costly and can be very complex due to the uneven geometry of the porous. To solve this issue, the equivalent macro models, operating based on the effective properties can be employed to avoid long computational time and find good quality results. Thus, this study aims at developing an equivalent porous model, which is much lighter than the previous ones [14], to describe the thermo-hydraulic behavior of the proposed RR porous medium using 3D microscale simulations and make validation by comparing the results at both levels, simulating Linear Fresnel (LF) solar applications.

The paper is organized as follows: the geometric characteristics of the porous medium and the solar receiver are presented in section 2, while section 3 provides the details of the numerical approach and shows the methodology used to achieve the equivalent model. The results of the micro and macro-scale studies are presented in section 4, and validation of the equivalent model is proposed. Later, the integration of the equivalent model for a case study is presented to approve the applicability of the presented approach for solar applications. Section 5 includes the main conclusions and summarizes the directions of the future works.

GEOMETRIC CHARACTERISTICS OF THE SOLAR RECEIVER

Solar Receiver

The tubular collector selected for the analyses is a conventional LS-2 tube used for PT and LF solar concentrators with dimensions of 66 mm inner diameter, and 70 mm outer diameter. A fraction of the tube with 21 cm length, consisting of 10 cm for upstream fluid (enough to be fully developed), 1 cm for the porous disc, and 10 cm for downstream fluid, is simulated and analyzed under three levels of fluid velocity within the macro and micro studies to provide a comprehensive understanding of the thermo-hydraulic behavior of the solar collector. For the case study, the solar heat flux is simulated based on literature [15] using a field function to model a LF solar collector with the concentration ratio of 58.36 which is employed with the secondary parabolic reflector. Fig. 1a represents the local concentration ratio (LCR) formulated to be applied to the solar collector. Taking into account the optical efficiency (η_{opt}) of 67% [15] and using a simplified heat loss coefficient (U_L) of 0.2 [13] with 1000 W/m^2 direct normal incident (DNI), the solar heat flux (Q_s) was given to the wall of tube as Eq. 1.

$$\boldsymbol{Q_s = DNI \times LCR \times \eta_{opt} \times (1 - U_L)} \quad (1)$$

RR Porous Medium

A novel porous disc with 10 mm thickness and 66 mm diameter consisting of RR in the orders of mm is designed and analyzed in this study. The material of the porous disc was selected as aluminum, and a detailed geometry including all individual rings was developed for the microscopic study, while in the macroscopic approach rings were replaced by an equivalent homogenous block formed with the same total volume and porosity.

NUMERICAL SIMULATION

A number of simulations were carried out based on a thermo-hydraulic model developed in the commercial Star CCM+ software implementing a three-dimensional analysis with steady-state, turbulent flow conditions. A steady-state conjugate heat transfer model was used to study the thermal behavior between solid and fluid regions. For the development of the macro model, micro-scale simulations were first performed under both hydraulic and thermodynamic approaches. Using the obtained data at this stage, macroscopic parameters such as inertia and viscous resistance, specific surface area, heat transfer coefficient between the fluid and solid porous materials, contact resistance, and other thermo-hydraulic characteristics were evaluated. Then, a new series of 3D simulations were performed based on the macroscopic details using LTNE and the same boundary conditions as micro-scale study. Considering the micro-scale study, the geometry of the porous disc was developed using Discrete Element Method (DEM) models. The detailed information about the procedure used for synthetic generation of random packing of the rings has been discussed in the previous works [14][18].

Microscopic Approach

Thanks to the symmetrical geometry and heating conditions in linear solar concentrating systems, microscopic simulations were developed for half of the pipe geometry to accelerate the convergence process and reduce computation costs. As shown in Fig. 1b, the computational domain was divided into the solid and fluid regions. The solid part, where a segregated solid energy equation is solved, consists of the tube geometry and the matrix of randomly positioned RR inside the tube. The fluid region was formed by boolean subtraction of the matrix structure from a cylindrical geometry filled inside the tube. Three levels of air velocity (0.6, 1, 1.4 m/s) were set at the inlet face of the fluid domain and the outlet face was arranged with a pressure boundary condition equal to 0 Pa. The intersection planes cutting all the computation domain into half were set as the symmetry plane, while the rest of the solid and fluid boundaries were set as wall boundaries. Also, a reference pressure of 10 bar was also applied to the system. In the case of hydraulic simulations, the no-heating condition was assumed to make pure pressure and velocity data for an accurate equivalent model (isothermal hydraulic characteristic). However, as far as the thermal analysis was concerned, heating was applied on the outer wall of the solid where several internal interfaces between the fluid and solid led to the transition of heat between regions. In order to simulate a turbulent flow inside the receiver, a two-equations Reynolds-Averaged Navier-Stokes (RANS) model, and namely the two-layer realizable κ-ε model, was used, with a two-layer wall treatment at the wall. The two-layer version of the κ-ε model adds flexibility to the wall treatment switching automatically between low-y+ and high-y+ treatments. As indicated by Dixon et al., [16], the superiority of the realizable κ-ε over the standard κ-ε model refers to the addition of an improved equation for the turbulent energy dissipation rate ε, with a variable viscosity coefficient C_μ instead of a constant value. Thus, as long as rotation boundary layers under strong adverse pressure gradients, separation, and recirculation with strong curvature are considered, similar to those found in packed tube simulation [17,18], this model could result in a reasonable performance. The realizable κ-ε model was also used and compared with k-ω model in the previous work [19], where results showed its applicability for simulation of RR porous inserts.

Microscopic Approach

Inertia and Viscous Resistance

According to the literature [6], when a gaseous fluid is passing through packed beds at high velocity, there is a non-linearity between the fluid flow rate and the driving pressure drop, and this increases the inertia effects. Therefore, under turbulence conditions, the Darcy law could not define the velocity field of fluid flow in porous medium and Darcy–Dupuit–Forchheimer model is introduced as in Eq. 2:

$$\frac{-\partial P}{\partial x_i} = \frac{\mu}{K} v_s + \rho C v_s^2 \quad (2)$$

where P, x, K, v_s, and C are respectively the fluid pressure, the direction of the flow, the permeability of the porous medium, inlet superficial velocity, and inertial factor. As described by [20], the values of the inertia (P_i) and viscous resistance (P_v) can be evaluated based on the pressure drop characteristics of the porous disc having a parabolic shape, which can be presented in the form reported in Eq 3.

$$\frac{-\partial P}{\partial x_i} = P_v v_s + P_i v_s^2 \quad (3)$$

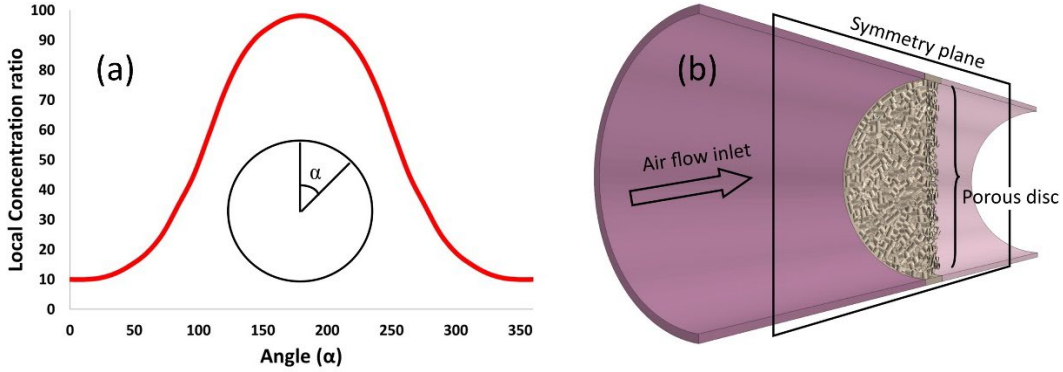

FIGURE 1. (a) Local concentration ratio on the absorber wall, (b) The outline of the solar absorber equipped with RR porous disc.

Heat Transfer Coefficient

To develop the equivalent model with volume-averaged thermal characteristics, a Local Thermal Non-Equilibrium (LTNE) model was added to the fluid domain as well as a multiphase interaction model including one solid and one phase interaction. Specific surface area (a_v), which is known as the ratio of total surface area (S_s) to the total volume (V_{tot}), was determined at the microscopic level and using Eq. 4 [9].

$$a_v = \frac{S_s}{V_{tot}} \quad (4)$$

The average heat transfer coefficient (HTC) between the fluid and solid rings was also determined through the microscopic study and applying a constant wall temperature (T_s=600 K) boundary condition to the rings. As a result, the other effective parameter needed for the equivalent model was found using the energy balance equation on the rings as reported in Eq. 5;

$$HTC = \frac{\dot{m} C_p (T_o - T_i)}{S_S (T_s - T_m)} \quad (5)$$

where T_o and T_i are the outlet and inlet temperatures of fluid, while T_m indicates the fluid mean temperature ($\frac{T_i + T_o}{2}$).

Grid

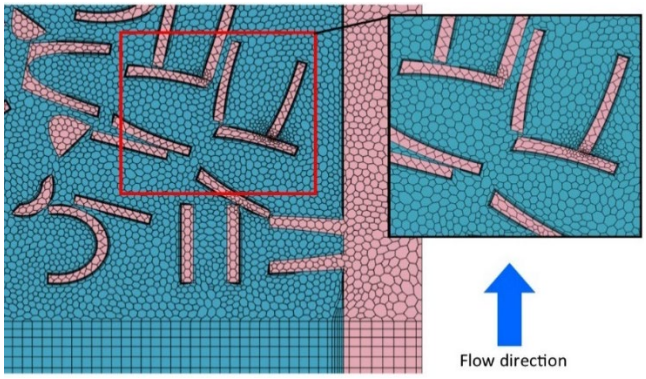

FIGURE 2. Mesh developed for the detailed simulations.

In the meshing stage and for the micro-scale study, polyhedral-based cells with a base size of 0.6 mm to a minimum limit of 0.06 mm were adopted in the RR region. The number of prism layers was set as 5 with y+ at the wall ~1 to make the model able to predict the sharp gradients on the wall boundaries. Inside the RR matrix the base size was reduced to 0.16 mm and the number of prism layers to 3. The portion of the plain pipe before and after the RR region was meshed extruding the mesh of the RR region. The result is a mesh based on prismatic cells with a polygonal base. As a result, more than 7.3 million cells were produced. Fig. 2 illustrates the structure of the mesh developed for simulations in this study, with particular emphasis on the RR region. However, in the macroscopic simulations, 0.3 million cells were generated, indicating a 96% reduction in the cells.

RESULTS AND DISCUSSION

Thermo-Hydraulics

In this section, numerical results of the detailed simulations are presented as the basis for the determination of effective properties used in the macroscopic study. The gradient of the pressure of the fluid along the porous medium at three different air velocities has been depicted in Fig. 3a. As expected, with an increase in Re number (air velocity), the pressure drop rises, reflecting a greater slope for the linear regression line. The values of these correlations were later used to plot the ratio of pressure drop over porous thickness ($\Delta P/L$) as a function of air velocity, reaching the Darcy–Dupuit–Forchheimer model as shown in Fig. 3b. The non-linear behavior of pressure drop is attributed to the addition of inertia effects that appear in turbulence flow. Therefore, the inertia and viscous resistance were extracted from the parabolic expression using Eq.3 to be used for the equivalent porous medium.

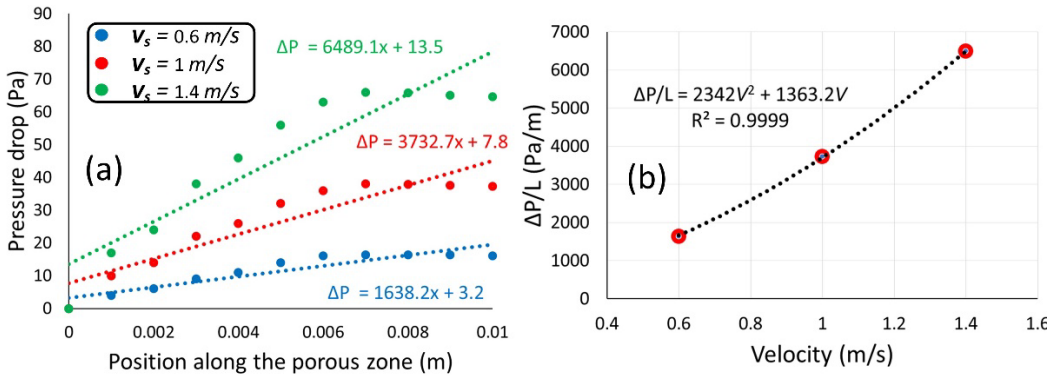

FIGURE 3. (a) Fluid pressure drops across the porous zone with respect to the position along the porous disc, (b) variations of pressure over the disc thickness with different superficial velocity.

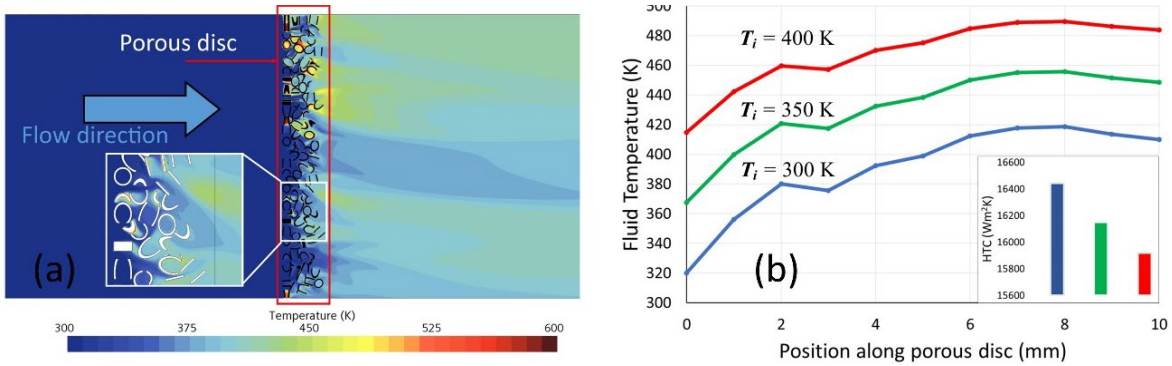

FIGURE 4. (a) Temperature development of air passing through a porous disc with constant RR surface temperature (Ts) of 600 K (Ti= 300 K), (b) Fluid temperature rise (averaged on the fluid surface sections) based on the constant RR surface temperature (Ts) and various air inlet temperatures (Ti) as well as the average heat transfer coefficient computed using CFD detailed simulations and Eq. 5, for Vs=1 m/s.

The detailed thermal behavior of the air passing through the porous disc, when the rings have the constant temperature of 600 K has been depicted in Figure 4a. It is clear that the integration of porous disc breaks the thermal boundary layers and promotes an enhanced heat transfer between the fluid and the solid part. The zoomed section also demonstrates the local effects of the position of rings on the thermal exchange and how the air streamlines could absorb heat from the wall of the rings. Fig. 4b indicates the average fluid temperature increase with respect to the movement inside the porous disc, with a range of inlet temperature and constant T_s. As it was expected, with the penetration through the medium, the fluid temperature rises where the maximum temperature is achieved at depth of 8 mm, which refers to the loose concentration of rings at the last 2 mm of the porous disc. Moreover, the average heat transfer coefficient (HTC) was obtained at each inlet temperature using Eq.5, where the maximum HTC was ~16500 W/m^2K for T_i= 300 K and the minimum value was measured as ~16000 W/m^2K for T_i= 400 K.

Validation of the Equivalent Results

Figure 5a represents a comparison of the fluid pressure drop obtained with macro and micro simulations using surface average values on the inlet and outlet faces of the porous disc. A very good agreement between the obtained values can be seen and this highlights the accuracy of the inertia and viscous resistance found in microscopic studies. Figure 5b provides the thermal performance of the porous medium using both microscopic and macroscopic approaches for the inlet temperature of 400 K, constant T_s= 600 K and the air velocity of 1 m/s. In the plot, the temperature profile of the macroscopic results is an averaged-volume representative of the fluid temperature in microscopic simulation. Moreover, the outlet temperatures obtained through both models are consistent and reflect a good agreement between the values. As shown in Fig. 5b, the temperature rise trend obtained in the micro study can be divided into three different zones. In the first zone, which is affected by the boundary, as the air enters the porous disc, the fluid temperature rises significantly due to the high temperature gradient between air and solid rings. Then in zone 2, the increase in the temperature difference becomes slower until it reaches a stable condition. Finally in zone 3 which is affected by the last porous layers, the solid and fluid reach the local thermal equilibrium and the temperature difference starts a downward trend.

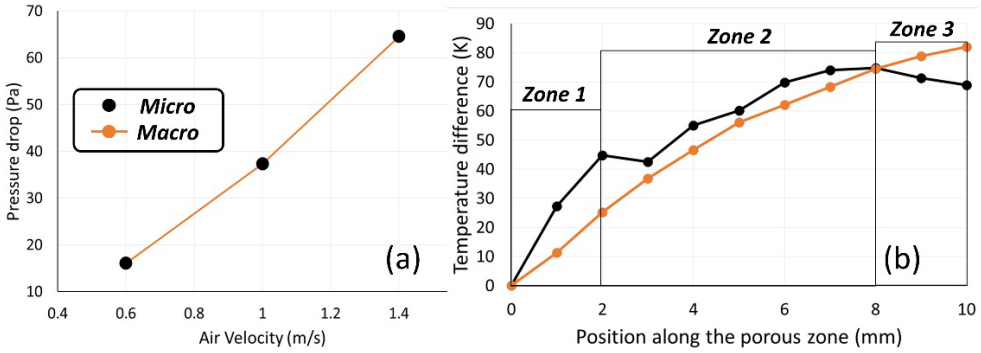

FIGURE 5. Comparison between the developed macro model and micro simulations (a) averaged fluid pressure drop versus air velocity, (b) average fluid temperature profile corresponding to the position inside the porous at V_s = 1 m/s and T_i = 400K.

Figure 6 shows the temperature map at three different cross-sections on the fluid direction inside the porous region. As shown, the temperature contours are different due to local effects considering in microscopic analysis. However, the development of temperature profiles is following the same pattern, representing the formation of high-temperature thermal layers adjacent to the tube wall with a similar gradient toward the core zone at both simulations. This also suggests that the macro model can predict the averaged-volume properties.

As it was well-observed in the detailed simulations, the improper contact between the tube wall and rings causes the thermal contact resistance, which is defined as the value of the resistance to conduction through the interface between rings and tube wall. To find the value of the contact resistance (R), simulations were performed under uniform heating ($\dot{q}$) on the wall of the tube at the micro-scale and the temperature difference on the interface between the tube (T_{s1}) and porous block (T_{s2}) was used to determine the thermal resistance as Eq. 6.

$$R = \frac{T_{s1} - T_{s2}}{\dot{q}} \tag{6}$$

As a result, the contact resistance was obtained as ~0.002 m^2K/W using both macro and micro simulations with a constant heat load of 250 kW/m^2 applied on the wall of the tube.

Figure 7 illustrates the comparison for the solid and fluid temperature profiles at the porous zone area and between the data obtained from macro and micro simulations under uniform heating. As shown in Fig.7a, the profile of the tube wall temperature obtained at the macro-scale study could be a good representative of average-volume temperature changes in the micro-scale with less than 0.5 K difference. Moreover, the air temperature profiles also show less than 3 K discrepancy in the average fluid temperature difference between the macro and micro simulations using the average heat transfer coefficient (Fig. 7b).

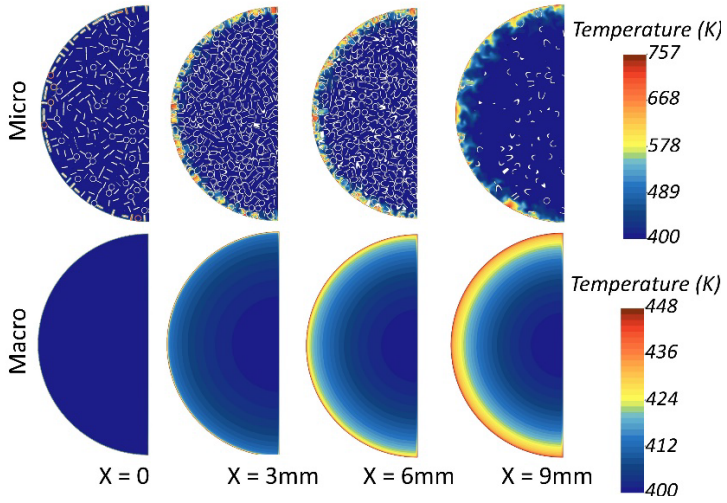

FIGURE 6. Temperature maps of the fluid passing through the porous disc with micro and macro analyses.

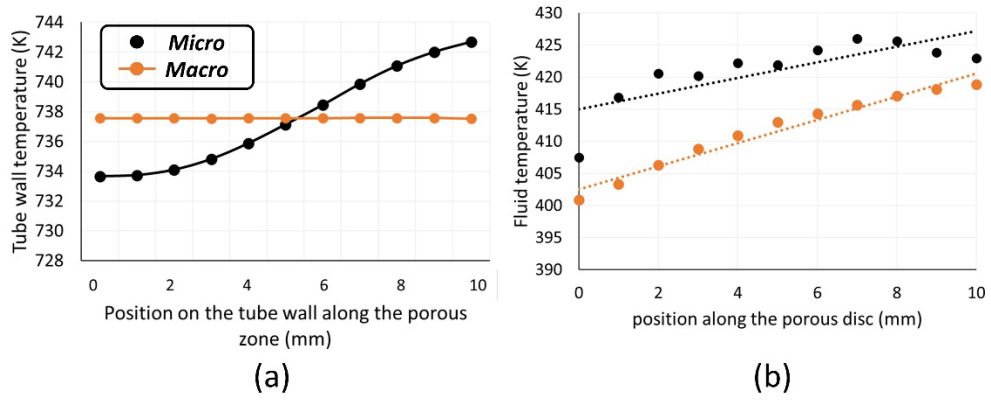

FIGURE 7. Comparison between the macro and micro model under uniform heat from the tube wall, (a) tube wall temperature, (b) Fluid temperature profiles.

LF Simulation with the Equivalent Model

Figure 8a depicts the temperature distribution on the wall of the receiver equipped with the porous disc using the developed micro model. As shown, the porous insert has resulted in a significant temperature reduction on the wall of the tube thanks to the higher heat transfer area and the thermal mixing that occurs inside the porous zone. Two hotspots are indicated to make a comparison between the peak values up and downstream. The temperature contours

demonstrate that the air leaving the porous zone has an enhanced heat transfer coefficient due to the turbulence induced in the fluid regime. Therefore, the second hotspot (Hotspot 2) does not reach the value of the first hotspot. Moreover, the reduction in the tube wall temperature is dominated in segments that receive the highest heat flux. As a result, the proposed porous disc can be used as a technique to reduce the heat loss that occurred between the tube and glass or ambient. According to Fig. 8b, the temperature rise on the tube of the tube wall has diminished by 40% compared to the case without porous disc. A lower tendency for temperature rise downstream is also representing the enhanced heat transfer coefficient achieved after passing through the porous. This proves that the proposed macro model could simulate the expected fluid flow and the turbulent effects occurring downstream.

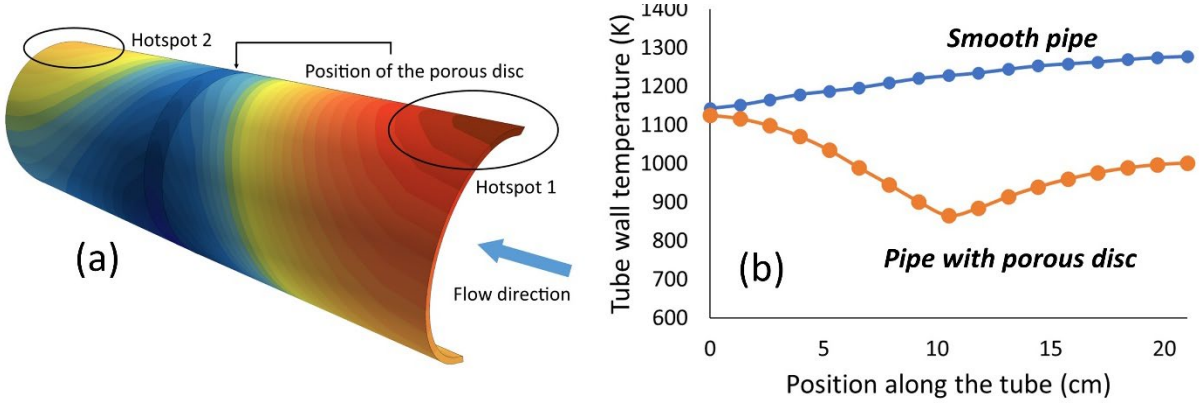

FIGURE 8. The application of the developed macro model to simulate a solar tubular absorber operating under LF heating (a) the temperature map of the tube wall, (b) comparison between the smooth pipe and the pipe quipped with RR.

CONCLUSION

The concept of using micro models to achieve an equivalent macro model for numerical CFD analysis was investigated in this study for a novel porous medium consisting of Raschig Rings. The comparison between the two simulations revealed that there is a good agreement between the results obtained, which proved the accuracy of the proposed method. Results also indicated that the macro model not only gives the hydraulic and thermodynamic parameters but also simulates the turbulent flow behavior for the air leaving the porous zone, which is very similar to that seen in micro-scale simulations. The average temperature differences obtained with micro-scale simulations reflected some fluctuations with respect to the position inside the porous zone, which shows the effects of the random positioning of the rings and non-uniform heat transfer between the rings and fluid along the flow direction. However, in macro-model, a smooth trend was observed rendering the volume-averaged properties used in the modeling. Employing the developed macro model for a linear Fresnel solar absorber showed that the porous insert could reduce the tube hotspot from >1200 K to <900 K, encouraging a reduced heat loss for solar absorbers. This study could be a cornerstone for future simulations to find the best optimum design of the absorber tube equipped with RR porous medium operating at CSP plants.

ACKNOWLEDGMENTS

We acknowledge the use of the computational resources provided by hpc@polito, which is a project of Academic Computing within the Department of Control and Computer Engineering at the Politecnico di Torino (http://hpc.polito.it).

REFERENCES

1. H. Rasam, P. Roy, L. Savoldi, and S. Ghahremanian, Energies **13**, (2020).
2. Varun, M.O. Garg, H. Nautiyal, S. Khurana, and M.K. Shukla, Renew. Sustain. Energy Rev. **63**, 193 (2016).
3. S. Gorjian, H. Ebadi, F. Calise, A. Shukla, and C. Ingrao, Energy Convers. Manag. **222**, 113246 (2020).

4. M.T. Jamal-Abad, S. Saedodin, and M. Aminy, Renew. Energy **107**, 156 (2017).
5. Z.-J. Zheng, M.-J. Li, and Y.-L. He, Appl. Energy **185**, 1152 (2017).
6. A.J. Otaru, Met. Mater. Int. **26**, 510 (2020).
7. T.P. de Carvalho, H.P. Morvan, D.M. Hargreaves, H. Oun, and A. Kennedy, Transp. Porous Media **117**, 311 (2017).
8. M. Cagnoli, A. Froio, L. Savoldi, and R. Zanino, Sol. Energy **190**, 195 (2019).
9. A.L. Avila-Marin, C. Caliot, G. Flamant, M. Alvarez de Lara, and J. Fernandez-Reche, Sol. Energy **162**, 317 (2018).
10. A. Sella, Chem. World **5**, 83 (2008).
11. L. Savoldi, F. Albajar, S. Alberti, K. Avramidis, A. Bertinetti, F. Cau, F. Cismondi, G. Gantenbein, J.-P. Hogge, and Z. Ioannidis, in *27th IAEA Fusion Energy Conf. - IAEA CN-258* (2018).
12. L. Savoldi, A. Allio, A. Bovento, M. Cantone, and J. Fernandez Reche, Sol. Energy (2020).
13. H. Ebadi, A. Allio, A. Cammi, and L. Savoldi, Am. Soc. Mech. Eng. Power Div. POWER **2021-July**, (2021).
14. H. Ebadi, A. Cammi, and L. Savoldi, in *19th Int. Conf. Renew. Energies Power Qual.* (Almeria (Spain), 2021).
15. E. Bellos and C. Tzivanidis, Sol. Energy **163**, 200 (2018).
16. A.G. Dixon, G. Walls, H. Stanness, M. Nijemeisland, and E.H. Stitt, Chem. Eng. J. **200**–**202**, 344 (2012).
17. E.M. Moghaddam, E.A. Foumeny, A.I. Stankiewicz, and J.T. Padding, Chem. Eng. J. **407**, 127994 (2021).
18. Y. Dong, B. Sosna, O. Korup, F. Rosowski, and R. Horn, Chem. Eng. J. **317**, 204 (2017).
19. A. Allio, R. Difonzo, A. Leggieri, F. Legrand, R. Marchesin, and L. Savoldi, Energies 2020, Vol. 13, Page 1163 **13**, 1163 (2020).
20. R. Nowak, Procedia Eng. **157**, 122 (2016).